Université de Liège

Faculté des Sciences appliquées
Département d'aérospatiale et mécanique

Nonlinear vibrations of aerospace structures

Referring professor: Gaëtan Kerschen

Nonlinear mechanical system analysis: from identification to simulation

François Ghysens - ID: s192059
Sven Michiels - ID: s195171
Alessandro Pase - ID: s2304388

Academic year 2023/2024

Contents

List of Figures

List of Tables

1. Introduction

1.1. Problem description

In the realm of mechanical and aerospace engineering, the prevalence of nonlinearities in structures has become increasingly apparent. This project aims to delve into the intricacies of nonlinear vibrations, using cutting-edge techniques within this specialized domain: the primary objective is to conduct a comprehensive analysis of an academic nonlinear mechanical system, progressing from initial measurements to a detailed understanding.
The focal point of the analysis is a two-degree-of-freedom (two-DOFs) system characterized by mass, linear damping and linear stiffness matrices. These matrices are known.
The key aspect of this system lies in the introduction of nonlinearities, the specific mathematical forms and coefficients of which are the object of the analysis. These nonlinear elements may manifest at any location within the system, adding an element of complexity to the study. The aim of this report is to unravel the nature of these nonlinear components, contributing not only to accurate results but also to a deeper understanding of their impact on the overall vibrational behavior of the system. Upon localizing the nonlinearity, a functional form will be sought through the application of the Acceleration Surface Method (ASM) and spectral analysis of the time response. Subsequently, the obtained form of this nonlinearity will be utilized in the Restoring Force Surface (RFS) method to estimate its coefficients. After fully characterizing the existing nonlinearities, the next step will involve the study of the non-linear system through the implementation of a shooting algorithm combined with a sequential continuation. Finally, the analysis will focus on the basins of attraction for the system with zero initial velocities of the structure near its two resonances. All implemented algorithms will be validated using experimental data and the *Nonlinear Identification to Design* (NI2D) software provided by the University of Liege.

1.2. System description

The matrices of mass, linear stiffness and linear damping, as anticipated, are known and are denoted as follows:

$$\mathbf{M} = \begin{bmatrix} 1 & 0 \\ 0 & 1 \end{bmatrix}, \quad \mathbf{C} = \begin{bmatrix} 3 & -1 \\ -1 & 3 \end{bmatrix}, \quad \mathbf{K} = \begin{bmatrix} 2 \times 10^4 & -1 \times 10^4 \\ -1 \times 10^4 & 2 \times 10^4 \end{bmatrix}$$

The system can therefore be represented as a two-degree of freedom mass-spring-damper system and can be schematized as in FIGURE 1.

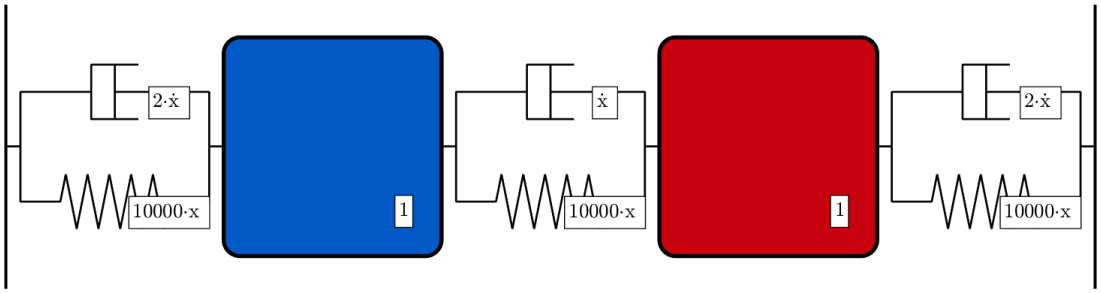

Figure 1: System diagram without nonlinearities (Source: NI2D)

The system, considered without nonlinearity, has two resonance frequencies equal to $f_1 = 15.915$ Hz and $f_2 = 27.566$ Hz, clearly visible in the frequency response functions (FRFs) of the linear system, represented in FIGURE 2.

The two modes of the system have a damping ratio of $\xi = 0.01$ for the first mode and $\xi = 0.0115$ for the second mode.

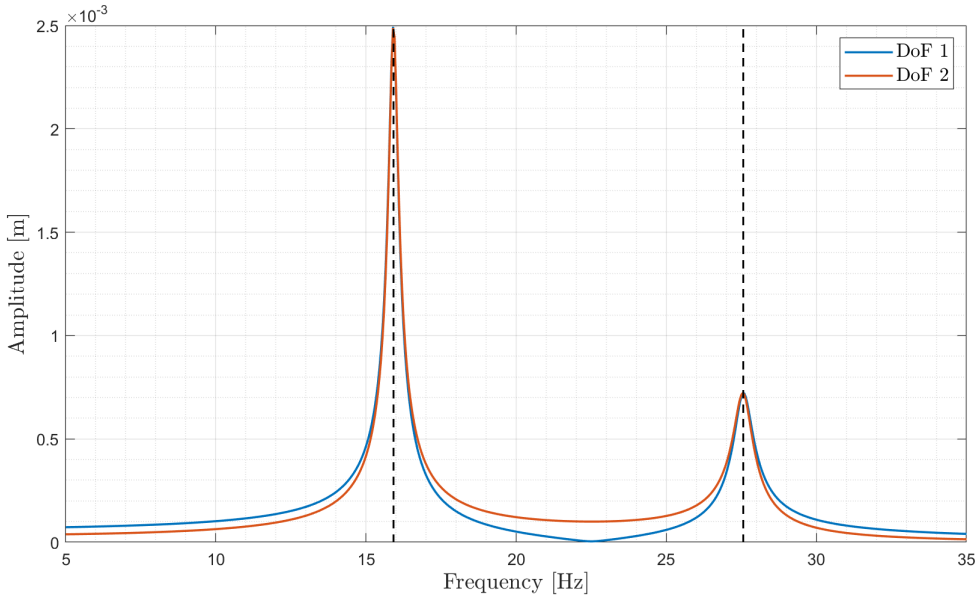

Figure 2: Frequency response functions for the linear system - Forcing amplitude: 1N on the DoF 1

2. Identification of the nonlinearities

2.1. Testing campaign

As previously mentioned, the system under analysis is only partially known and its study involved testing the system to obtain results. Specifically, in this project, there were five opportunities to simulate the experiment, considering up to three different types of forces for each experiment. Each experiment yields the displacement, velocity and acceleration of each degree of freedom as output. The parameters used for each experiment conducted in this study are provided in the APPENDIX A, for completeness.

2.2. Detection of the nonlinearities

2.2.1. Sinesweep time response analysis

Detecting nonlinear behavior is the initial step in identifying the structure's nonlinearities. To accentuate these potential nonlinearities, numerous tests were conducted during the testing campaign (refer to APPENDIX A). Within this campaign, a deliberate choice was made to employ a linear sine sweep excitation. This specific excitation effectively stimulates nonlinear behaviors by concentrating energy across all frequencies in the bandwidth of interest. This deterministic signal also simplifies visual data interpretation.
Frequency Response Function (FRF) analysis provides a clear method for detecting structural nonlinearities. The simplest approach involves comparing the structure's linear FRF with its FRF when nonlinearities are active. This comparison is established by simulating an equivalent system with matrices M, C and K, excited by the same input signal using NI2D software and is represented on FIGURE 3. The data used to make the comparison is the one from the first test of experiment 3. The parameters for this simulation are summarized in Tab 5.

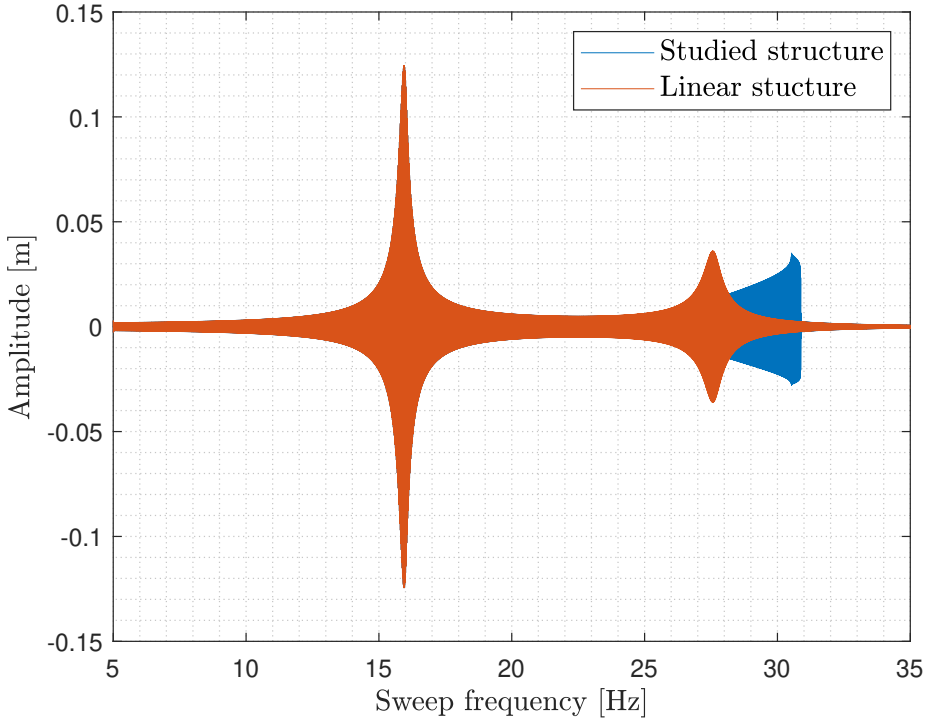

Figure 3: Comparison between the frequency response function of the linear structure and the real structure of Dof 2 - Forcing amplitude: 50N on the DoF 1

As seen in FIGURE 3, the comparison between the linear case and the activated nonlinearities case reveals a distinct difference in the FRFs around the second resonance frequency. Indeed, the FRFs coincide accurately at the first resonance frequency of 15.91 Hz. However, closer examination around 27.57 Hz exposes disparities between the curves. Notably, a significant shift is observed in the FRFs with activated nonlinearities, transitioning from 27.5 Hz to 30.5 Hz. This pronounced shift serves as an initial indication of the structure's nonlinear behavior. Moreover, notable characteristics within the nonlinear FRFs further affirm the structure's nonlinear behavior. A significant amplitude jump close to 30.3 Hz highlights the nonlinear behavior of the structure. Additionally, the observed stiffness increase approaching the second resonance frequency substantiates the presence of nonlinear behavior. The asymmetry in amplitude variation surrounding the second resonance frequency also plays a role in highlighting the structure's nonlinear behavior.
Another approach to detect the nonlinearities in the structure is to make a comparison between different FRFs of the structure. The comparison involves comparing nonlinear FRFs excited by different excitation signals. The comparison will be done between nonlinear FRFs with different directions for the sine sweep excitation (sweep up and down) and is represented in FIGURE 4.

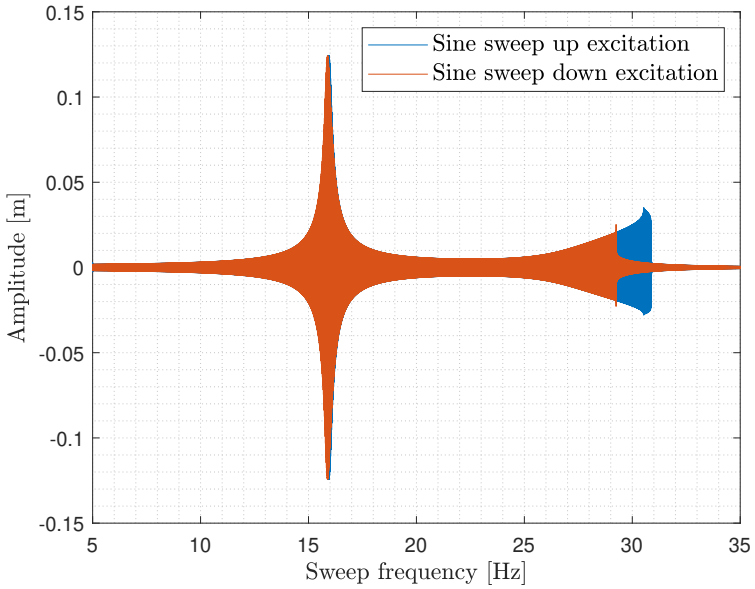

Figure 4: Comparison between the frequency response function of a sine sweep up and down excitation of Dof 2 - Forcing amplitude: 50N on the DoF 1

In FIGURE 4, noticeable disparities are evident in the FRFs. These discrepancies primarily stem from the direction of the sine sweep excitation, particularly evident around frequencies close to the structure's second resonance frequency. For each FRF, the nonlinear characteristics discussed previously are retrieved such as sudden jumps in amplitude, increased stiffness near the resonance frequency and asymmetry along the x-axis. Nevertheless, the FRFs do not have the same shape whether the structure is excited with a sine sweep up or a sine sweep down of equivalent amplitude. This discrepancy is another fact that the structure behaves nonlinearly. However, note that a difference could also be noticed around the frequencies close to the first resonance frequency as it was observed for tests 1 and 2 of experiment 2 (cf.FIGURE 5).

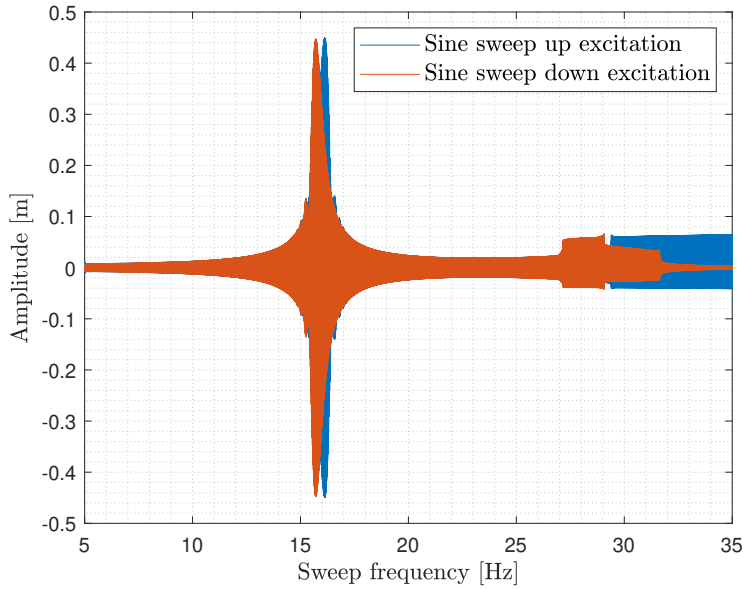

Figure 5: Comparison between the FRF of a sine sweep up and down excitation of Dof2. Experiment 2 test 1 and 2

This variation in the Frequency Response Functions (FRFs) does not stem from the nonlinear characteristics of the structure but rather arises from the transient effects within the structure's response. It is noteworthy that the FRF analysis assumes a steady-state condition, while the utilization of a sinesweep disrupts this assumption, introducing a minor shift in the results. Consequently, this deviation can be attributed to the transient nature induced by the sinesweep, rather than inherent nonlinearities in the structural behavior.
Another approach is analyzing the Frequency Response Functions (FRFs) across various amplitudes of excitation to reveal the structural nonlinearity. For linear structures, FRFs should maintain a consistent appearance with only amplitude variations. By comparing FRFs obtained at different amplitudes during sine sweep excitations, differences become apparent. This comparison is illustrated in FIGURE 6.

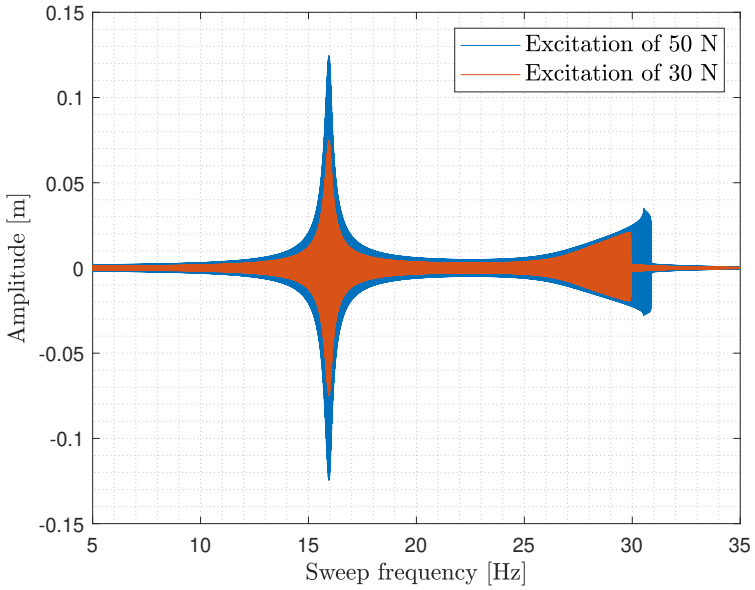

Figure 6: Comparison between the FRF of a sine sweep for different forcing amplitude on Dof 2.

Distinct variations emerge in the FRF shapes for different amplitude excitations, particularly near the second resonance frequency where nonlinearities manifest. Indeed, the shift observed in frequency is smaller for smaller amplitude excitation. This observation further solidifies the understanding that the structure exhibits nonlinear behavior.

2.2.2. Localisation of the nonlinearity

The identification of the structure's nonlinear behavior allowed for localizing the nonlinearities within the structure. As previously discussed, these nonlinearities were notably present near the second resonance frequency while being absent near the first resonance frequency. This observation plays a crucial role in determining the location of the nonlinearities within the structure.
Considering a linear two-degree-of-freedom system, where each of the two masses is interconnected with the other via springs and dampers, and also individually connected to the ground through their respective springs and dampers, the first mode of vibration is an in-phase motion of the two masses, meaning that the relative displacement between the masses is equal to zero. This means that the influence of the interconnecting springs and dampers between the masses is negligible in this specific mode of motion since they are not solicited.
In our specific system, if the nonlinearities were localized between one mass and the ground, we would expect to see differences in the FRFs at the first vibration mode when comparing the linear structure (without nonlinearities) to the studied structure (with nonlinear behavior). However, the absence of any distinction in the FRFs at the first resonance frequency implies that the nonlinearities likely exist between the two masses rather than between an individual mass and the ground.

2.3. Characterization of the nonlinearities

Having identified and localized the nonlinearities within the structure, the next step involves characterizing these nonlinear behaviors. The characterization will be done using a commonly employed method which is the Acceleration Surface Method (ASM) enabling to characterize the damping and stiffness curve related to the nonlinearities in the system. Another characterization method which will be used is the analysis of the harmonic content of the signal using the Continuous Wavelet Transform (CWT).

2.3.1. Acceleration surface method (ASM)

In the context of systems with multiple degrees of freedom, the ASM method assumes that nonlinearities can be represented by concentrated elements —such as lumped springs and dashpots— located at specific points where the nonlinear behavior is localized, as depicted in Figure 7.

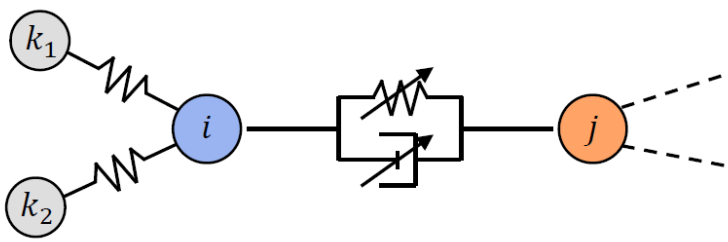

Figure 7: Assumption of the Acceleration Surface Method (ASM)

This method considers the simplified representation of the system based on Newton's Second Law for a degree of freedom i:

$$\sum_k m_{i,k}\ddot{q}_k + g_i(q,\dot{q}) = p_i$$

The ASM simplifies this equation by discarding terms unrelated to the nonlinear connection, assumes no forcing term and omits the mass constant, leading to:

$$g_i(q_i - q_j, \dot{q}_i - \dot{q}_j) \cong -\ddot{q}_i$$

In essence, this approach enables a comprehension of nonlinearities by examining how acceleration varies concerning both relative velocity and displacement. The nonlinearities, represented as a spring and damper, depend on both relative displacement and velocity in their function. To visualize the specific nonlinear damping effect, the function must exclusively rely on relative velocity. This involves plotting acceleration with respect to relative velocity while maintaining a relative displacement of zero, ensuring the function isolates the influence of relative velocity. Similarly, to demonstrate the effect of nonlinear stiffness, the function should solely rely on relative displacement. This requires plotting acceleration against relative displacement while keeping the relative velocity at zero, focusing the function solely on relative displacement within the nonlinearities' analysis. This approach provides valuable insights into the configurations of the stiffness and damping curves, aiding in the parametrization of nonlinearities. However, it's important to note that while the Acceleration Surface Method (ASM) assists in identifying the functional form of the parameters, it does not facilitate the direct estimation of their values. The acceleration surface and the stiffness curve obtained using the ASM method are represented on FIGURES 8a & 8b. The acceleration surface and the damping curve are shown in FIGURES 9a & 9b.

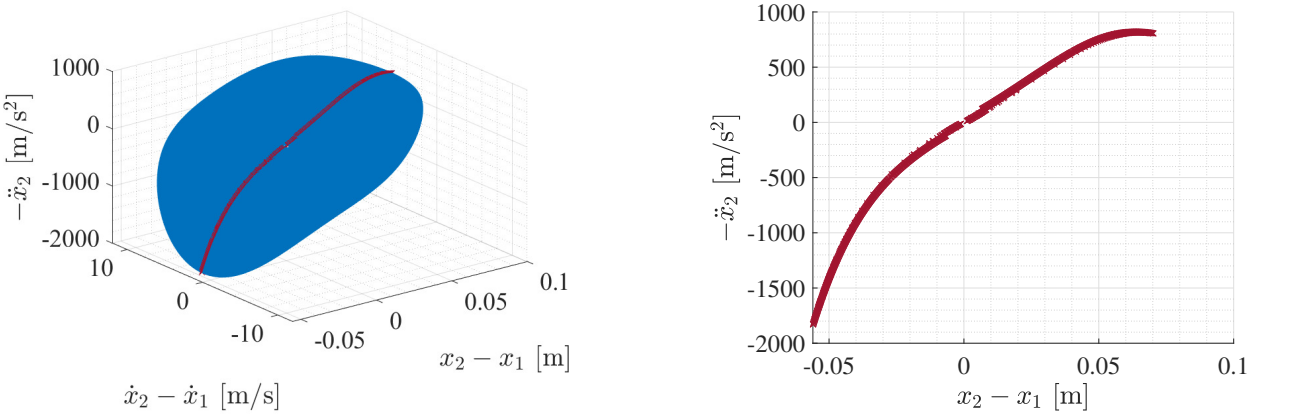

(a) Acceleration surface at Dof 2 and acceleration for zero velocity (in red).

(b) Evolution of the negative absolute acceleration at Dof 2 concerning the relative displacement

Figure 8: Acceleration surface and stiffness curve for Dof 2. Experimental data from test 1 of experiment number 3.

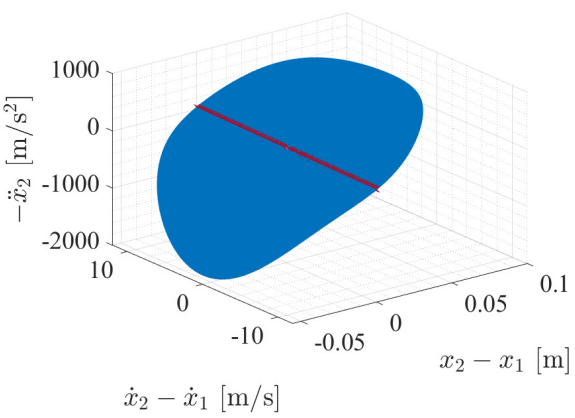

(a) Acceleration surface at Dof 2 and acceleration for zero displacement (in red).

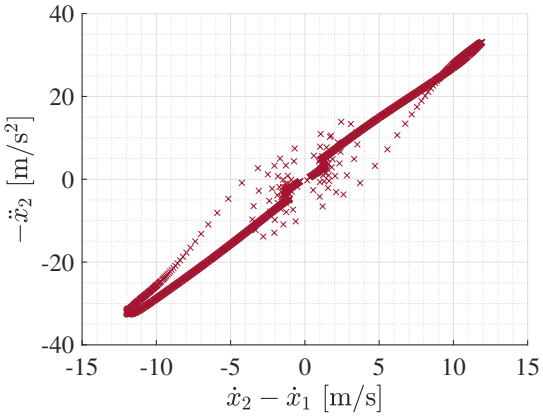

(b) Evolution of the negative absolute acceleration at Dof 2 concerning the relative velocity

Figure 9: Acceleration surface and damping curve for Dof 2. Experimental data from test 1 of experiment number 3.

In FIGURES 8b and 9b, the relative displacement and velocity chosen originate from test 1 within experiment 3. This specific test enables clear visualization of nonlinearities, with a shift below 30% from the initial second resonance frequency. This shift allows for a more precise examination of the nonlinear behaviors.
The selection of relative displacement and velocity focuses on the frequency range where the nonlinearities manifest in the FRFs, particularly near the second resonance frequency. The absolute acceleration is chosen from Degree of Freedom (Dof) 2 within the same frequency range. This choice conforms to the assumption in the ASM that no external forcing acts on this Dof, as the excitation force is applied to Dof 1.
Upon examining the stiffness and damping curves using the ASM, it is evident that the stiffness curve can be closely approximated by a polynomial function, since it is smooth and without discontinuities. Another thing that can be noticed is the asymmetry of the stiffness curve, which suggests the use of polynomials not strictly even. The damping curve, instead, appears more fitting for a linear function. The small magnitude of acceleration attributed to damping force, in comparison to that arising from the stiffness force, suggests that the linear damping curve implies the absence of nonlinear damping force. It further indicates that the sole nonlinear force present is a stiffness force located between the two degrees of freedom. Additionally, several points lying outside the predominant region exhibit characteristics resembling a hysteresis curve if included in the analysis. However, for accuracy, these points are disregarded. They originate from the excitation signal's impact on the nonlinearity, which ideally wouldn't influence the identification of damping and stiffness curves: typically, to precisely identify these curves, nonlinearities should not be stimulated. Yet, in the case of this analysis, as the nonlinearities exist between the two masses, there is no choice but to stimulate them during the analysis.

2.3.2. Harmonics analysis with Continuous Wavelet Transform (CWT)

In signal processing, the Continuous Wavelet Transform is a mathematical tool used for analyzing the frequency content of signals. Unlike the Discrete Fourier Transform (DFT), which uses fixed sinusoidal basis functions, the CWT employs wavelets that are localized in both time and frequency. This allows for a more flexible representation, making it well-suited for analyzing signals with non-stationary or time-varying characteristics. To enhance visualization, the maximum value of the colorbar has been constrained to 800, ensuring that even the narrowest harmonics remain visible. The choice of the signal was made with computational efficiency in mind, given that processing a response with a sweep rate of 1 Hz/min would have been impractical due to the overwhelming number of data points involved.

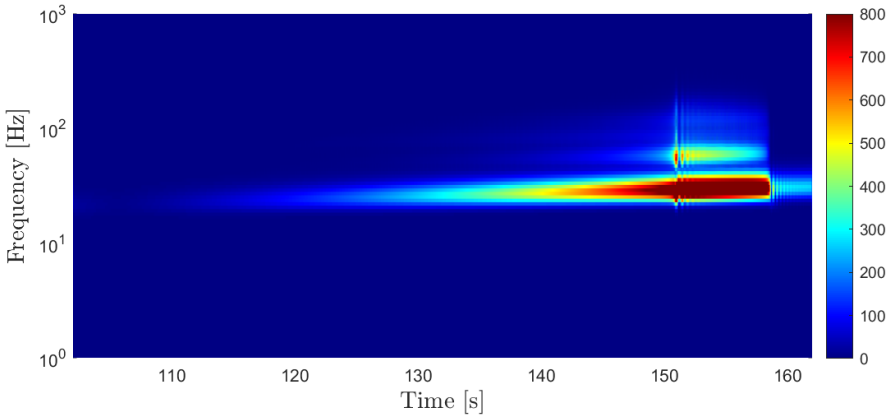

Figure 10: Continuous Wavelet Transform of sinesweep response of the system - Experiment 2, test 3

By employing the Continuous Wavelet Transform for the analysis of harmonic content, valuable insights can be obtained to characterize nonlinearity and formulate hypotheses regarding its functional form. Notably, the absence of jumps in the transform aligns with the smoothness emphasized by the Accelerated Surface Method (ASM), suggesting a lack of discontinuities in the nonlinear force. Additionally, the identification of even harmonics, specifically the 2nd and 4th harmonics, indicates the presence of asymmetric nonlinearities. It is worth noting that the experimental data, sourced from numerical simulations, remain free from harmonic content induced by measurement noise.

2.4. Parameter estimation

The process involves parameterizing nonlinearities, utilizing the Restoring Force Surface (RFS) method based on Newton's second law for a multi-degree-of-freedom system. In our case, the equations governing the system are given by

$$\mathbf{M}\ddot{\mathbf{q}} + \mathbf{C}\dot{\mathbf{q}} + \mathbf{K}\mathbf{q} + \mathbf{f}_{nl}(\mathbf{q}, \dot{\mathbf{q}}) = \mathbf{f}_{ext}$$

where $\mathbf{f}_{ext}$ is the external force applied to the system and $\mathbf{f}_{nl}$ is the nonlinear force acting on the system and that depends on the displacement $\mathbf{q}$ and velocity $\dot{\mathbf{q}}$ at both degrees of freedom. The nonlinear force characterizing the nonlinearities can thus simply be expressed as

$$\mathbf{f}_{nl}(\mathbf{q}, \dot{\mathbf{q}}) = \mathbf{f}_{ext} - \mathbf{M}\ddot{\mathbf{q}} - \mathbf{C}\dot{\mathbf{q}} - \mathbf{K}\mathbf{q}$$

The RFS can be used for nonlinear parameter estimation if one assumes a functional form for $\mathbf{f}_{nl}$ which is obtained from nonlinear characterization. More precisely, the estimated nonlinear force is given by

$$\hat{\mathbf{f}}_{nl} = \sum_{i=1}^{M} k_i \mathbf{f}_i(\mathbf{q}, \dot{\mathbf{q}})$$

where the terms $\mathbf{f}_i$ represent the functional form of the nonlinear force that have been deduced from the stiffness and damping curve from the acceleration surface method. The restoring force surface method is then used to compute the coefficients k_i multiplying the different assumed functional forms of the nonlinear force. The aim is to find the coefficients such that the estimated nonlinear force $\hat{\mathbf{f}}_{nl}$ corresponds to the actual measured nonlinear force $\mathbf{f}_{nl}$. Using the measurements of the displacement $\mathbf{q}$, velocity $\dot{\mathbf{q}}$ and acceleration $\ddot{\mathbf{q}}$ of both degrees of freedom at the Q measurement times, a system of equations for the coefficients k_i is obtained under the

form;

$$\begin{bmatrix} \mathbf{f}_1(\mathbf{q}(t_1),\dot{\mathbf{q}}(t_1)) & \cdots & \mathbf{f}_M(\mathbf{q}(t_1),\dot{\mathbf{q}}(t_1)) \\ & \vdots & \\ \mathbf{f}_1(\mathbf{q}(t_Q),\dot{\mathbf{q}}(t_Q)) & \cdots & \mathbf{f}_M(\mathbf{q}(t_Q),\dot{\mathbf{q}}(t_Q)) \end{bmatrix} \begin{bmatrix} k_1 \\ \vdots \\ k_M \end{bmatrix} = \begin{bmatrix} \mathbf{f}_{ext}(t_1) - \mathbf{M}\ddot{\mathbf{q}}(t_1) - \mathbf{C}\dot{\mathbf{q}}(t_1) - \mathbf{K}\mathbf{q}(t_1) \\ \vdots \\ \mathbf{f}_{ext}(t_Q) - \mathbf{M}\ddot{\mathbf{q}}(t_Q) - \mathbf{C}\dot{\mathbf{q}}(t_Q) - \mathbf{K}\mathbf{q}(t_Q) \end{bmatrix}$$

which can be solved as a least-squares problem for which the solution is given by;

$$\begin{bmatrix} k_1 \\ \vdots \\ k_M \end{bmatrix} = \begin{bmatrix} \mathbf{f}_1(\mathbf{q}(t_1),\dot{\mathbf{q}}(t_1)) & \cdots & \mathbf{f}_M(\mathbf{q}(t_1),\dot{\mathbf{q}}(t_1)) \\ & \vdots & \\ \mathbf{f}_1(\mathbf{q}(t_Q),\dot{\mathbf{q}}(t_Q)) & \cdots & \mathbf{f}_M(\mathbf{q}(t_Q),\dot{\mathbf{q}}(t_Q)) \end{bmatrix}^{\dagger} \begin{bmatrix} \mathbf{f}_{ext}(t_1) - \mathbf{M}\ddot{\mathbf{q}}(t_1) - \mathbf{C}\dot{\mathbf{q}}(t_1) - \mathbf{K}\mathbf{q}(t_1) \\ \vdots \\ \mathbf{f}_{ext}(t_Q) - \mathbf{M}\ddot{\mathbf{q}}(t_Q) - \mathbf{C}\dot{\mathbf{q}}(t_Q) - \mathbf{K}\mathbf{q}(t_Q) \end{bmatrix}$$

Based on the results of the acceleration surface method, the nonlinear force is assumed to be a polynomial function depending on the relative displacement $q_2 - q_1$. The damping curve exhibiting a linear behavior of the acceleration with respect to the relative velocity $\dot{q}_2 - \dot{q}_1$, it can be concluded that the nonlinear force does not depend on the relative velocity. Furthermore, as stated previously, the nonlinear force is assumed to be located between both degrees of freedom and does not depend on the displacement or velocity of a single degree of freedom and only depends on the relative displacement between both degrees of freedom.
To find the right coefficients of the nonlinear force and the order of the polynomial expression of the nonlinear force being unknown, the order of the polynomial was gradually increased until the estimated nonlinear force corresponded to the actual nonlinear force. To do so, the functional forms $\mathbf{f}_i$ were expressed as

$$\mathbf{f}_i = \begin{bmatrix} -(q_2 - q_1)^i \\ (q_2 - q_1)^i \end{bmatrix}.$$

The force acting on each node has an opposite sign such that the sum of the nonlinear forces acting on the two degrees of freedom is equal to 0. Indeed, since the force is located between the two masses, it is a force internal to the system and the sum of all the internal forces of a system has to be equal to 0. The experimental results used for this parameter estimation were those of the first test of the third experiment.
After increasing the order of the polynomial up to the 7th order, the estimated nonlinear force seemed to correspond very accurately to the measured nonlinear force. Increasing the order of the polynomial did not further improve the estimation of the nonlinear force. It was thus concluded that the expression of the nonlinear force was a polynomial of order 7 of the relative displacement between both degrees of freedom. Furthermore, as the coefficients of the terms of order 1, 2, 5 and 6 were very small compared to those of order 3,4 and 7, they were disregarded in the parameter estimation, such that only the terms of order 3, 4 and 7 were retained. The expression of the nonlinear force was thus found to be equal to

$$\hat{\mathbf{f}}_{nl} = \begin{bmatrix} -2.1 \times 10^{10}\ (q_2 - q_1)^7 + 5.3 \times 10^7\ (q_2 - q_1)^4 - 2.5 \times 10^6\ (q_2 - q_1)^3 \\ 2.1 \times 10^{10}\ (q_2 - q_1)^7 - 5.3 \times 10^7\ (q_2 - q_1)^4 + 2.5 \times 10^6\ (q_2 - q_1)^3 \end{bmatrix}.$$

The nonlinear force as a function of the relative displacement for zero initial velocity and as a function of the relative velocity for zero relative displacement are illustrated in Figure 11.
It can be seen that the expression of the nonlinear force obtained with the RFS method corresponds to the measured nonlinear force. From Figure 11b, it can be observed that the nonlinear force does not follow a specific trend compared to the relative velocity and that the measured values are very small. The hypothesis that the nonlinear force does not depend on the relative velocity can thus be considered to be valid.

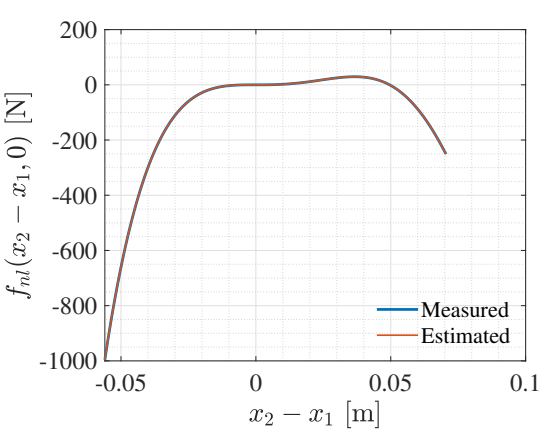

(a) Nonlinear force as a function of the relative displacement for zero relative velocity.

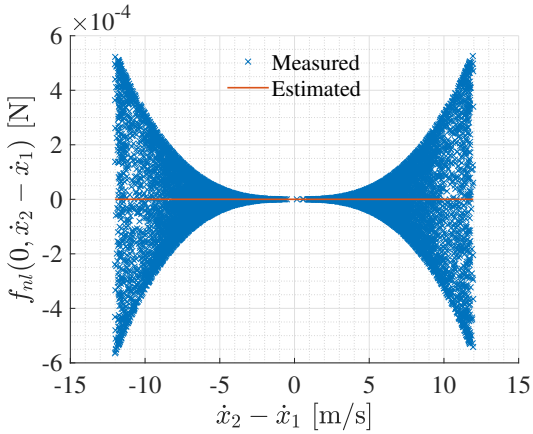

(b) Nonlinear force as a function of the relative velocity for zero relative displacement.

Figure 11: Measured and estimated nonlinear force at degree of freedom 2 as a function of relative displacement and relative velocity.

To further verify the validity of the expression of the nonlinear force, the response to a sine force with an amplitude of 30 N at frequencies of 10 Hz and 30 Hz simulated on the NI2D software is compared to experimental results. These two forcing frequencies have been chosen in order to represent the response at a frequency where the system behaves linearly, namely at 10 Hz, and at a frequency where the system is clearly nonlinear, which corresponds to the frequency of 30 Hz. The results are depicted in FIGURES 12a & 12b.

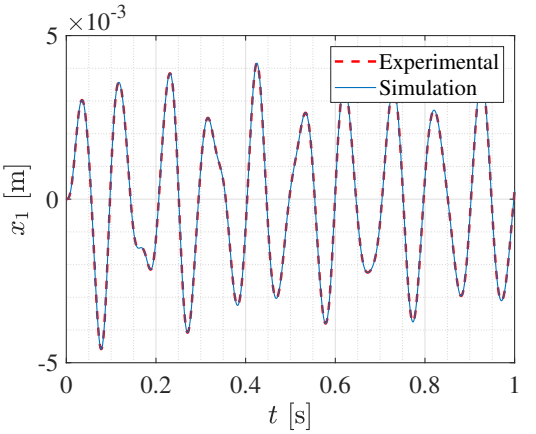

(a) Forcing frequency of 10 Hz. Experimental data from test 3 of experiment 5.

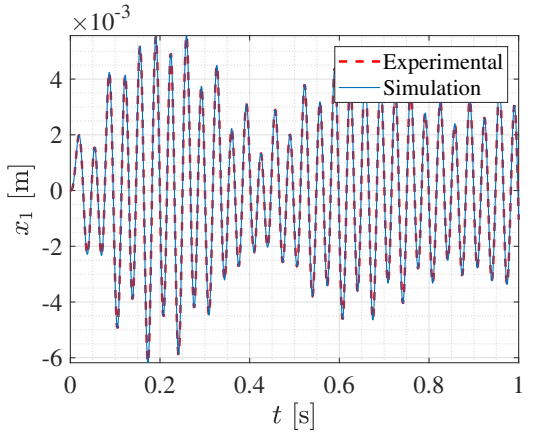

(b) Forcing frequency of 30 Hz. Experimental data from test 3 of experiment 5.

Figure 12: Comparison between the experimentally measured response and the time response with the estimated nonlinear force - zoom on the transient.

As can be seen, the simulated results obtained using the estimated expression of the nonlinear force exactly correspond to those measured experimentally. This gives an additional confirmation for the expression of the nonlinear force that has been obtained.

3. Simulation of the non-linear system

In this chapter, numerical methods for simulating nonlinear systems will be examined and their potential implementation will be presented. All methods have been subsequently implemented in MATLAB and the system under study will be simulated, highlighting its peculiarities. The entire process will then be validated using the NI2D software and the obtained experimental data.

3.1. Frequency Response Curves (FRCs) computation

3.1.1. Shooting algorithm

One of the peculiarities of nonlinear systems is their strong dependence on initial conditions. Unlike linear systems, the presence of a periodic response in the system is contingent upon the specific initial conditions imposed on the system.
The shooting algorithm is a numerical method used to solve initial value problems (IVPs) for ordinary differential equations (ODEs). This algorithm, in the context of nonlinear simulation, is implemented to determine the initial conditions that, for each frequency, ensure the presence of a purely periodic response in the system.
The algorithm has been implemented in MATLAB following the logic presented in Figure 13.

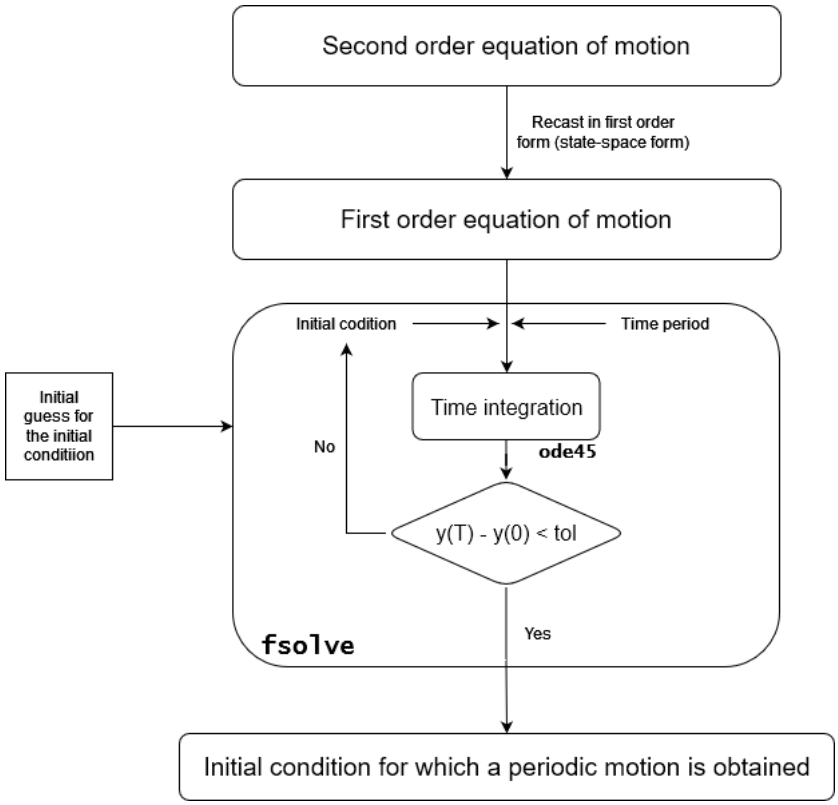

Figure 13: Shooting algorithm flowchart.

The shooting algorithm employs the built-in MATLAB function **fsolve** to find the zero of the function $\mathbf{h} = \mathbf{y}(T; \mathbf{y_{0,p}}) - \mathbf{y_{0,p}}$. The function to find the zero is thus the difference between the solution of the time integration after one oscillation period, with the only variable being the initial condition itself. The period is calculated as the reciprocal of the frequency for which the solution is sought. The phase of numerical time integration, as often encountered, is a sensitive aspect of the process and has undergone thorough investigation. Two solutions were explored within the project, assessing their respective merits and drawbacks. Initially, a

Newmark integration algorithm tailored for nonlinear systems was implemented from scratch. Subsequently, its performance was evaluated by comparing it with MATLAB's built-in **ode45** algorithm, which relies on an adaptive Runge-Kutta scheme.
In terms of solution, no substantial differences were observed, affirming the correctness of the implemented algorithm. However, as anticipated, MATLAB's native algorithm (ode45) proved significantly more efficient, enhancing computational times. This difference holds particular importance, especially within the continuation algorithm, where the shooting process is repeated numerous times.
To employ "ode45" in solving the motion equation, it was necessary to express the equations in state-space form, thereby reducing the order while increasing the number of unknowns, as expressed in the following equations.

$$\dot{\mathbf{y}}(t) = \mathbf{L}\mathbf{y}(t) - \mathbf{g}_{nl}(\mathbf{y}) + \mathbf{g}_{ext}(\omega, t)$$

With:

$$\mathbf{y} = \begin{bmatrix} \mathbf{x} \\ \dot{\mathbf{x}} \end{bmatrix}; \qquad \mathbf{L} = \begin{bmatrix} \mathbf{0} & \mathbf{I}_n \\ -\mathbf{M}^{-1}\mathbf{K} & -\mathbf{M}^{-1}\mathbf{C} \end{bmatrix};$$

$$\mathbf{g}_{nl} = \begin{bmatrix} \mathbf{0} \\ \mathbf{M}^{-1}\mathbf{f}_{nl}(\mathbf{x}, \dot{\mathbf{x}}) \end{bmatrix}; \quad \mathbf{g}_{\text{ext}} = \begin{bmatrix} \mathbf{0} \\ \mathbf{M}^{-1}\mathbf{f}_{\text{ext}}(\omega, t) \end{bmatrix}.$$

Another aspect that requires attention is the tolerances, both those imposed on "ode45" and those on "fsolve": given the small amplitude oscillations, stringent tolerances are necessary. However, a trade-off must be carefully evaluated to avoid excessively burdening the computational cost.

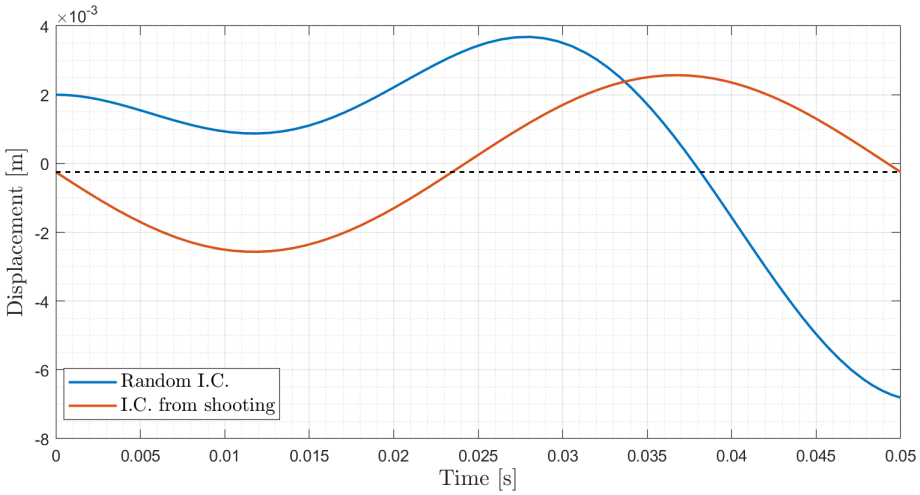

Figure 14: Impact of the initial condition on the periodic motion - F = $sin(2\pi 20t)$ on DoF 1.

3.1.2. Sequential continuation algorithm

The shooting algorithm was implemented and utilized to obtain Frequency Response Curves (FRCs) through the application of a continuation algorithm. The continuation algorithm employs the shooting algorithm to obtain initial conditions at various oscillation frequencies, calculating the amplitude of periodic oscillation at each frequency. In this project, a sequential-type continuation algorithm was implemented. In each iteration, there is a sequential increment in ω, calculating the next point on the FRC. While this type of continuation has the advantage of simplicity in implementation, it has certain limitations. The primary limitation is the significant challenge in continuing beyond the turning point.

As mentioned, nonlinear FRCs exhibit more complex shapes than linear FRFs, owing to factors such as the presence of multiple stable solutions for certain frequencies. The sequential algorithm, lacking consideration for curve characteristics such as its tangent, encounters difficulty in adequately tracking the curve, particularly after the turning point. This limitation hinders its ability to capture all possible solutions.
In the presence of turning points, the occurrence of discontinuities or "jumps" in response curves is expected. These points correspond to sudden changes in the system's dynamics, often associated with transitions between different stable solutions. The sequential continuation algorithm, due to its limitations in addressing turning points, may not be able to fully and accurately capture these discontinuities in the response curve. In such situations, more advanced continuation strategies such as the pseudo-arclength scheme, may be necessary to obtain reliable and comprehensive results.
To capture as many parts of the Frequency Response Curves (FRCs) as possible, the continuation algorithm was implemented in such a way that if the "fsolve" function takes numerous iterations to converge, the calculation stops and restarts from the last frequency of interest with a negative $\Delta\omega$. This is based on the observation that, when convergence is challenging, the solution at $\omega + \Delta\omega$ is often significantly distant from the solution at ω, given that the initial guess is precisely the previous solution.

3.1.3. Frequency Response Curves (FRCs) of the nonlinear system

With the algorithms previously described, the nonlinear system under analysis was simulated, yielding various Frequency Response Curves (FRCs) at different forcing amplitudes. The simulated frequency range is $[5, 45]$ Hz to comprehensively capture all features of the obtained curves. The system was simulated by varying the force amplitude between 10 N, 30 N and 50 N to emphasize the significant differences, both in terms of shape and magnitude, exhibited by the Frequency Response Curves (FRCs) of a nonlinear system. The results are depicted in Figure 15.

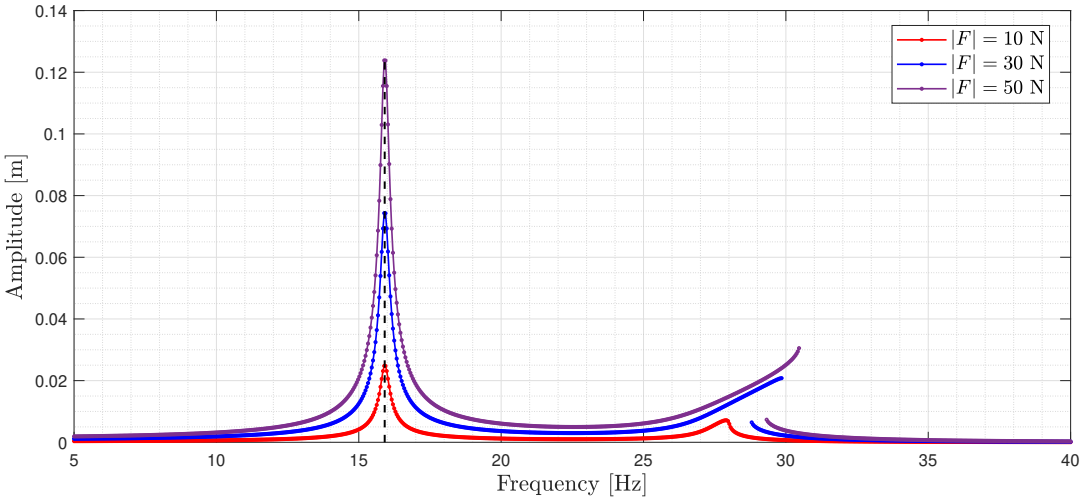

Figure 15: FRC of the DOF 2 for three different forcing amplitude on DOF 1.

It can be observed that the shape of all the Frequency Response Curves (FRCs) around the first resonance frequency of the linear system precisely corresponds to the shape of the linear Frequency Response Function (FRF). This confirms what has been explained and demonstrated in Section 2: since the nonlinearity is only present between the two degrees of freedom of the first mode, characterized by in-phase motion, it remains entirely linear.
On the other hand, the second mode, as highlighted earlier, is nonlinear. With a force amplitude

of 10 N, the nonlinearity is barely noticeable, with only a slight bending of the resonance peak observed. However, with an increased forcing amplitude of 30 N or 50 N, the nonlinear nature of the response becomes more apparent. Increasing the force magnitude leads to obtaining Frequency Response Curves (FRCs) with the presence of a turning point, highlighting the limitation of the sequential continuation algorithm. When encountering a turning point, the continuation fails, resulting in a jump in the curve. This jump will be analyzed in Section 3.1.4.

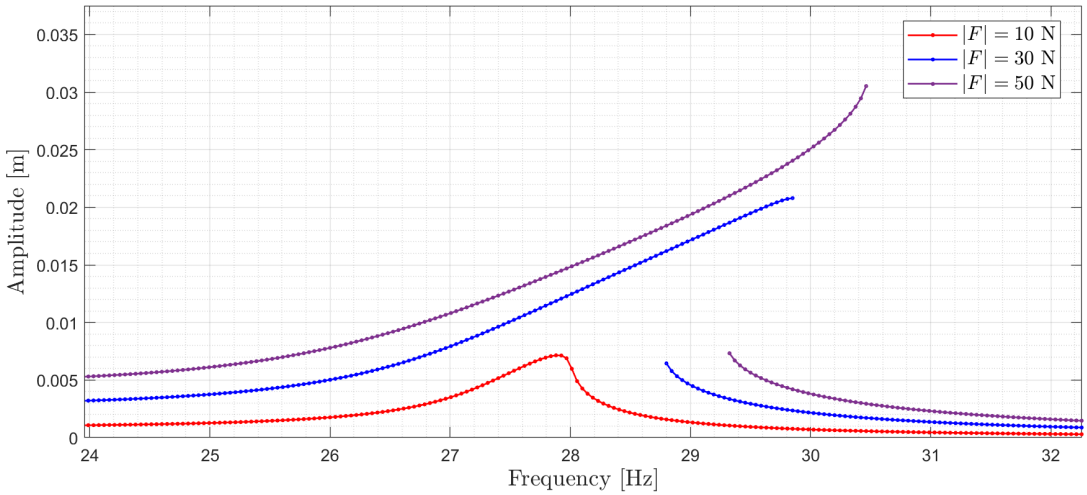

Figure 16: FRC of the DOF 2 for three different forcing amplitude on DOF 1 - zoom around the second resonance peak.

3.1.4. Validation of the continuation algorithm

The continuation algorithm implemented during the project has been validated to confirm its correctness. For validation, both the NI2D software, which internally incorporates a harmonic balance continuation algorithm and the time response of the system using a sinesweep as the forcing function, were used as benchmarks.

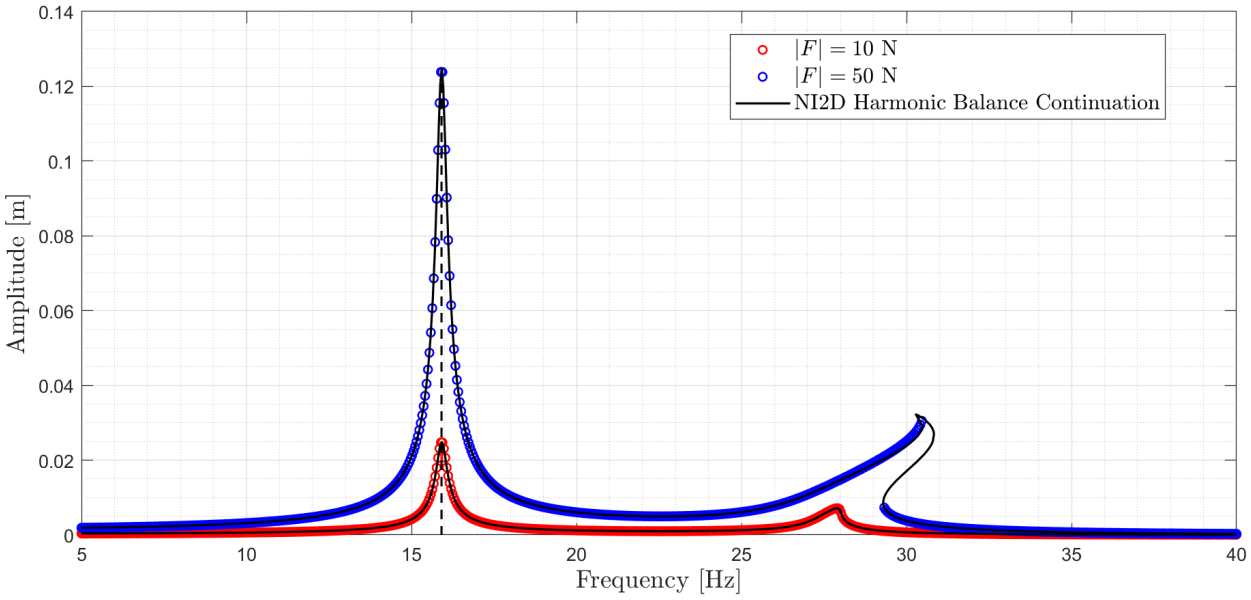

Figure 17: Comparison between the implemented algorithm and the NI2D software - Amplitude of DOF 2 with a Force on DOF1.

It can be observed that the implemented algorithm works correctly, within the mentioned limitations of the sequential continuation. The two curves perfectly overlap until the turning point, where the NI2D software, employing a more refined algorithm, manages to follow the curve. Notably, for a force amplitude of 50 N, the Frequency Response Curve (FRC) exhibits a distinctive double bending, indicating an initial hardening and subsequent softening of the nonlinear stiffness. However, the self-made algorithm halts at the first turning point, restarting from the last frequency backward and subsequently encountering another blockage. For a force amplitude of 10 N, the obtained curve is identical to that calculated by the NI2D software, since there are no turning points. Another confirmation of the effectiveness of the implemented algorithm is evident when overlaying the system's response to a sinesweep-type forcing function. This type of force, besides being useful in identification, can be employed to analyze Frequency Response Curves (FRCs). The sinesweep effectively forces the system across all frequencies within the area of interest, with the amplitude of these oscillations equal to the amplitude of the FRC at that given frequency.

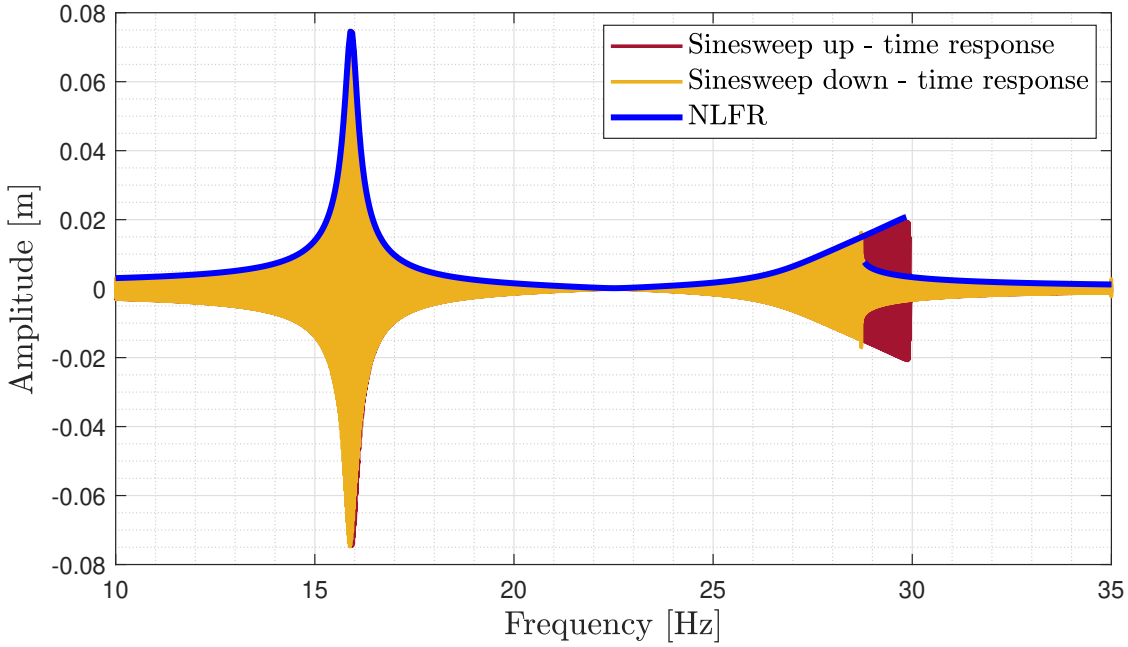

Figure 18: Superposition of the sinesweep response of the first DOF and the NLFR - Experiment 4 Test 2 & 3.

It can be observed in FIGURE 18 that, in this case as well, the algorithm behaves as expected, accurately simulating the amplitude of the oscillations. Special attention should be given to the discontinuity: there is a clear distinction in behavior when considering a sinesweep up or a sinesweep down. With a positive sweep rate, the system will follow the upper branch of the FRCs and, at the first turning point, switch branches to follow the other solution. With a negative sweep rate, the solution will exhibit the opposite behavior, following the lower branch until the turning point, then making a jump to switch to the other branch.

3.2. Nonlinear Normal Modes (NNMs) computation

Nonlinear normal modes are a concept used to describe the periodic, natural vibrational modes of nonlinear systems. Unlike linear normal modes, the amplitudes of nonlinear normal modes may not scale linearly with the excitation amplitude. Analyzing nonlinear normal modes is more complex than linear normal modes due to the nonlinearity of the system. Nonlinear systems can exhibit behaviors such as amplitude-dependent frequencies and mode coupling, which are not present in linear systems. The Nonlinear Normal Modes are useful because

they describe the deformation at resonance of the structure and how the modal parameters evolve with motion amplitude. To highlight the frequency-amplitude dependence of nonlinear oscillations, the most effective tool is the backbone curve. To obtain the backbone curve, the previously introduced continuation algorithm is applied to the undamped and unforced system.

3.2.1. Frequency-energy plot (FEP)

A useful graphical representation of the frequency-amplitude dependence is the Frequency-Energy Plot (FEP). This plot is obtained by calculating, from the initial conditions obtained through the shooting algorithm, the total energy associated with the motion, which is equal to the initial potential energy in the case of an undamped and unforced system without non-conservative forces. In the examined system, the initial potential energy as a function of initial conditions is calculated as follows.
Defining:

$$\begin{bmatrix} A & B & 0 & 0 \end{bmatrix} = \begin{bmatrix} q_1(0) & q_2(0) & \dot{q}_1(0) & \dot{q}_2(0) \end{bmatrix}$$

The energy associated with the linear elements can be expressed as:

$$E_{linear} = V_{linear} = \frac{A^2}{2} + \frac{B^2}{2} + \frac{(B-A)^2}{2}$$

while the potential associated with the nonlinear springs can be expressed as:

$$\begin{aligned} E_{nonlinear} = V_{nonlinear} &= \int_0^{B-A} \mathbf{f}_{nl} \, \mathrm{d}(x_2 - x_1) \\ &= \frac{2.1 \times 10^{10} \, (B-A)^8}{8} - \frac{5.3 \times 10^7 \, (B-A)^5}{5} + \frac{2.5 \times 10^6 \, (B-A)^4}{4} \end{aligned}$$

Therefore the potential energy is:

$$V = V_{linear} + V_{nonlinear}$$

Given that the in-phase mode is linear, its oscillation amplitude is independent of frequency, unlike the second out-of-phase mode. The out-of-phase mode is strongly nonlinear, as evident from the significant dependence of oscillation energy on the frequency of the oscillation. Once again, the limitation of the sequential algorithm is apparent, as it fails to find solutions beyond the first turning point.

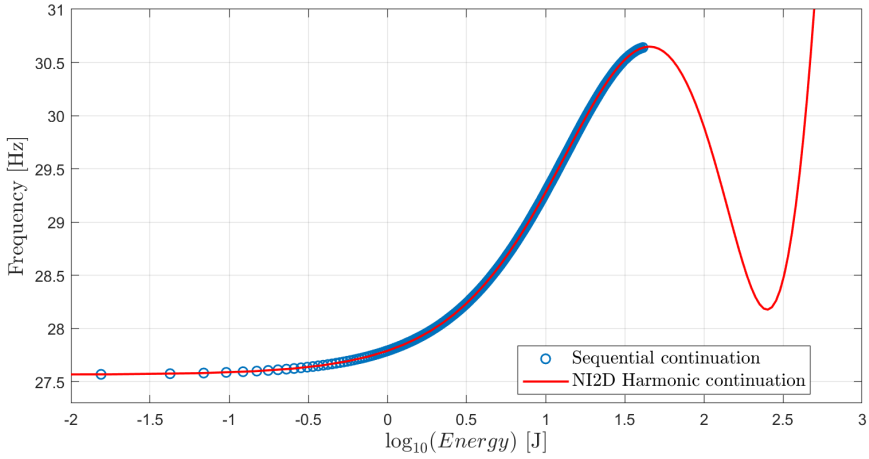

Figure 19: Frequecy energy plot (FEP) - Implemented sequential continuation vs NI2D continuation.

3.2.2. Backbone curve computation

As anticipated, another useful tool for the analysis of Nonlinear Normal Modes is the backbone curve. This curve represents the evolution of the oscillation amplitude as the frequency varies. The backbone curve is obtained by once again utilizing the continuation algorithm combined with shooting, applied to the undamped and unforced system. Similar to the frequency-energy plot, the backbone curve has been calculated for the second mode, where the nonlinearities are present.

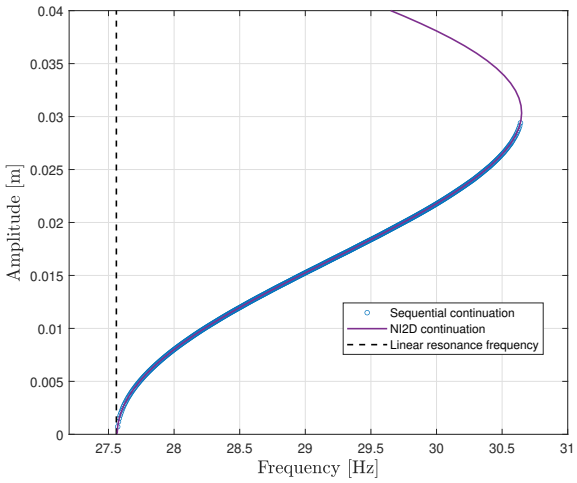

Figure 20: Comparison between the backbone curve obtained with sequential continuation and the one obtained with the aid of NI2D.

Once again, the obtained curve can be validated by referring to the result from the NI2D software. It is noticeable that the two curves perfectly overlap until the turning point.
A critical aspect to emphasize when calculating Nonlinear Normal Modes (NNMs) and the backbone curve concerns the initial conditions. This type of calculation is extremely sensitive to the initial guesses and must be chosen with care. The starting point of the backbone is known: at the resonance frequency of the linear system, the amplitude is zero. However, starting from this point would cause the shooting process to fall into the trivial solution, consistently returning null values. Another observation pertains to the phase of the two degrees of freedom: when studying the second mode of vibration, as in the present case, an initial guess out-of-phase should be chosen for correct convergence.

3.2.3. Link between the backbone curve and the FRFs

The term "backbone curve" is used because, considering Frequency Response Curves (FRCs) at different force levels, it represents the backbone of these FRFs. It is possible to overlay the calculated backbone with the FRFs obtained for various values of forcing amplitudes.
The pattern of the backbone curve aligns with the trends observed in the Frequency Response Curves (FRCs) at varying forcing amplitudes for both degrees of freedom. Notably, the intersection points between the backbone and the FRCs at 10 N and 30 N coincide with the peaks of the FRCs. However, the absence of a Frequency Response Curve at 50 N is notable. This discrepancy arises because, at this specific forcing amplitude, the sequential continuation method fails to accurately capture the peak of the FRCs due to a double bend, a characteristic discernible only through the results obtained via NI2D. The leftward bending can also be inferred from the tangent of the FRC just before the continuation algorithm halts: the tangent to the FRC is nearly vertical, suggesting a change in direction towards the left.

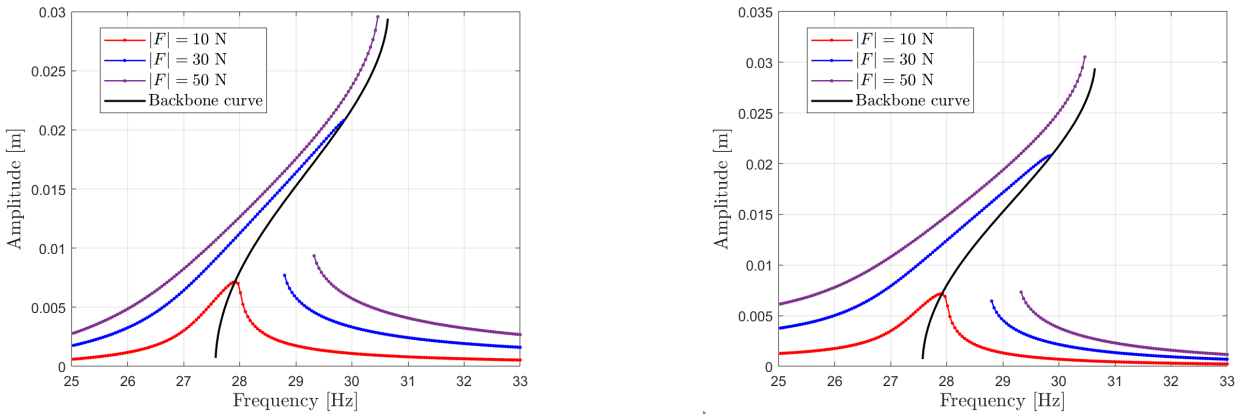

(a) Degree of freedom: 1

(b) Degree of freedom: 2

Figure 21: Superposition of the NNM backbone curve to NLFRs at three different forcing levels.

3.3. Basins of attractions

As previously mentioned, for a fixed set of parameters, solutions of a nonlinear system may not be unique and, unlike linear systems, the solution can be stable or unstable. To gain insights into the stability of the solution, one can employ stability analysis for discrete-time mechanical systems. One option involves linearizing the system and utilizing the Floquet theory to assess the stability of the solution.

The analysis of basins of attraction plays a pivotal role in understanding the behavior of dynamic systems, providing valuable insights into how different initial conditions influence the long-term evolution of a system. In the realm of dynamical systems theory, a basin of attraction represents a region in the phase space wherein specific initial conditions lead the system towards a particular attractor.

The analysis was conducted at a forcing frequency of $f = 28.8$ Hz and $f = 29.5$ Hz, at which, as evident in FIGURE 22, two distinct stable solutions are present. The analysis was also performed, for confirmation, at the frequency $f = 15$ Hz, close to the resonance frequency of the first mode. At this frequency, a uniform region is expected since multiple solutions are not present.

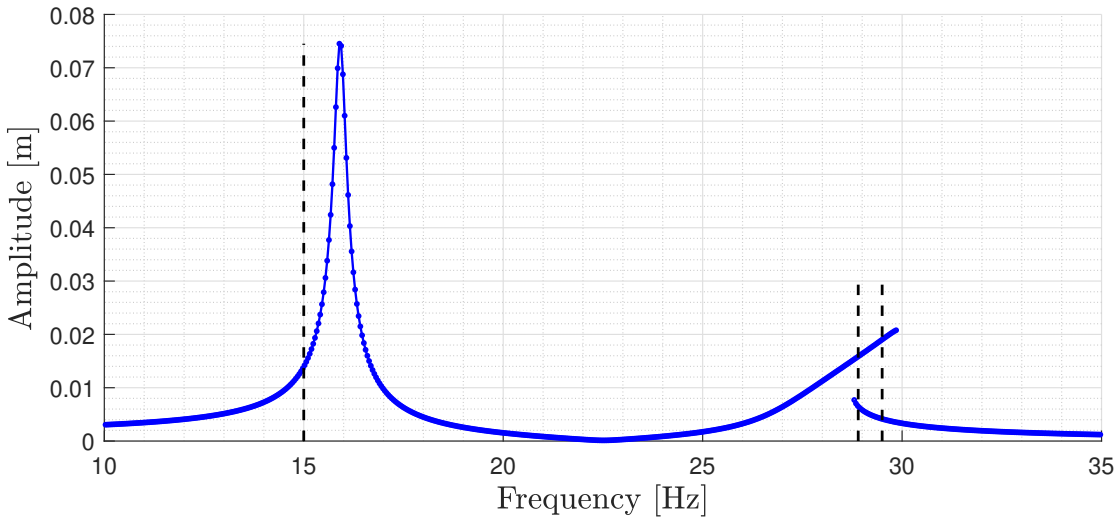

Figure 22: Frequency response curve at 30 N - DOF 1

The time response also strongly depends on the initial conditions regarding velocity. For the sake of visualization, the analysis was conducted by fixing the initial velocity to zero and varying the amplitude of $x_{0,1}$ and $x_{0,2}$ within the interval [-0.15, 0.15].

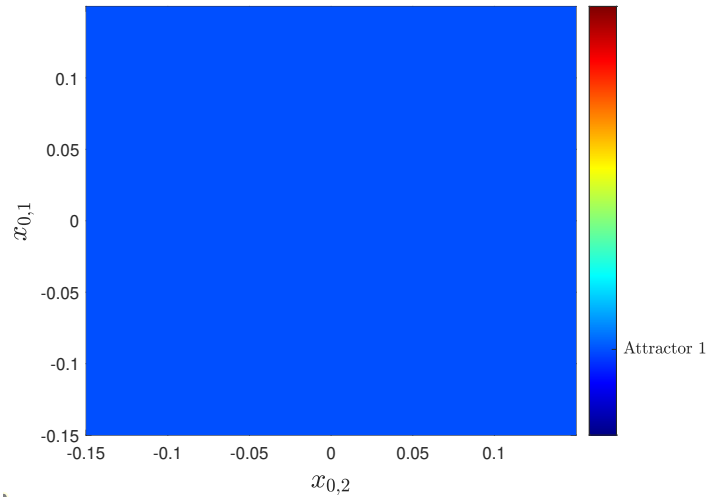

Figure 23: Basins of attractions - Forcing amplitude: 30N, forcing frequency: 15 Hz

The analysis confirmed what one might expect: for the frequency close to the first resonance, the solution converges to a single attractor. This is evident in FIGURE 22 & 23, where no multiple solutions are observed with an excitation frequency of 15 Hz.

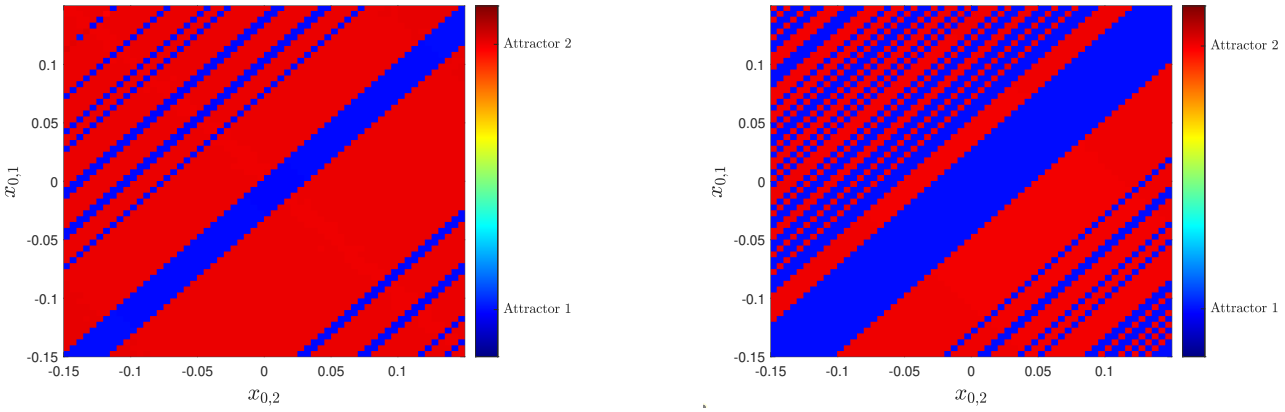

(a) Forcing frequency: 28.8 Hz

(b) Forcing frequency: 29.5 Hz

Figure 24: Basins of attractions - Forcing amplitude 30N

For the second analyzed frequency, instead, there are two stable solutions. The shape of the attractors illustrates how the converging solution is highly dependent on both initial conditions in a manner not describable with a univocal relation. It can also be noted that the shape of the regions strongly depends on the excitation frequency. Small variations in frequency lead to distinct regions, as highlighted in FIGURE 24.
The configuration does not exhibit the conventional "spiral" pattern found in other basin of attraction plots. This deviation arises because, in contrast to those cases, the two initial conditions undergoing variation are the initial displacements, not both the initial displacement and initial velocity of the same degree of freedom. It is worth observing that the figure displays a checkered pattern, a consequence of limitations in resolution due to the prohibitively high computational cost. Given N distinct initial conditions for $x_{0,1}$ and N for $x_{0,2}$, the algorithm necessitates $N \times N$ time-integrations.

4. Conclusions

During this project on the analysis of a nonlinear mechanical system, all the characteristics of nonlinear systems have been highlighted, starting from detection, proceeding with identification and concluding with numerical methods to simulate such nonlinear systems.

Although the detection of nonlinearity may not be inherently complex, considerable attention has been dedicated to this step in this analysis. In academic or industrial contexts, it is a key factor in deciding whether to invest in the complex and resource-intensive study of nonlinearities. For this phase, the importance of using a sinesweep forcing excitation has been emphasized, as it allows the activation of all frequencies of interest during an experiment. Analyzing the responses to this type of excitation has enabled the observation of key features of nonlinear systems, such as the presence of jumps in the response, shifts in the resonance peak and a strong frequency-amplitude dependence.
After highlighting the presence of nonlinear forces and localizing them between the two degrees of freedom (DOFs), which corresponds to an out-of-phase movement generating relative displacement of the two masses, it has become possible to characterize the system as a whole.

Once the presence of nonlinearity in the system was confirmed and localized, the system was characterized by first analyzing its possible functional form using the Acceleration Surface Method (ASM) aided by the Continuous Wavelet Transform (CWT), allowing the estimation of a polynomial functional form. Subsequently, using the Restoring Force Surface (RFS) method, the coefficients were obtained through a Least-Squares fit, resulting in the following expression for the nonlinear force:

$$\hat{\mathbf{f}}_{nl} = \begin{bmatrix} -2.1 \times 10^{10}\ (q_2 - q_1)^7 + 5.3 \times 10^7\ (q_2 - q_1)^4 - 2.5 \times 10^6\ (q_2 - q_1)^3 \\ 2.1 \times 10^{10}\ (q_2 - q_1)^7 - 5.3 \times 10^7\ (q_2 - q_1)^4 + 2.5 \times 10^6\ (q_2 - q_1)^3 \end{bmatrix}.$$

Furthermore, it was observed through the above-mentioned tools that there is an absence of dependence on relative velocity, allowing the consideration of purely linear damping.

After obtaining a complete characterization of the system, numerical methods for simulating these types of systems were analyzed, highlighting the capabilities and limitations of the sequential continuation algorithm. All implemented algorithms were validated using the NI2D software as a high-fidelity model. In the final step, the presence of double stable solutions within these types of systems was analyzed by exploring the basins of attractions while varying the initial conditions on displacement.

A. Testing parameters

A.1. Experiment number: 1

	Test 1	**Test 2**	**Test 3**
Type	Sine sweep	Sine sweep	Sine sweep
Forced dof(s)	1	1	2
Amplitude [N]	400	400	300
Starting frequency[Hz]	5	35	5
Ending frequency [Hz]	35	5	35
Phase	-	-	-
Sweep rate [Hz/min]	10	10	10
Sweep style	linear	linear	linear
Number of repetitions	-	-	-

Table 1: **External force** parameters for experiment number 1

	Test 1	**Test 2**	**Test 3**
Time step [s]	1.4e-4	1.4e-4	1.4e-4
Initial time [s]	0	0	0
Duration [min]	3	3	3

Table 2: **Newmark solver** parameters for experiment number 1

A.2. Experiment number: 2

	Test 1	**Test 2**	**Test 3**
Type	Sine sweep	Sine sweep	Sine sweep
Forced dof(s)	1	1	1
Amplitude [N]	200	200	100
Starting frequency[Hz]	5	45	5
Ending frequency [Hz]	45	5	45
Phase	-	-	-
Sweep rate [Hz/min]	10	10	10
Sweep style	linear	linear	linear
Number of repetitions	-	-	-

Table 3: **External force** parameters for experiment number 2

	Test 1	**Test 2**	**Test 3**
Time step [s]	1.1 10e-4	1.1 10e-4	1.1 10e-4
Initial time [s]	0	0	0
Duration [min]	4	4	4

Table 4: **Newmark solver** parameters for experiment number 2

A.3. Experiment number: 3

	Test 1	**Test 2**	**Test 3**
Type	Sine sweep	Sine sweep	Sine sweep
Forced dof(s)	1	1	1
Amplitude [N]	50	10	5
Starting frequency[Hz]	5	5	5
Ending frequency [Hz]	45	45	45
Phase	-	-	-
Sweep rate [Hz/min]	1	1	1
Sweep style	linear	linear	linear
Number of repetitions	-	-	-

Table 5: **External force** parameters for experiment number 3

	Test 1	**Test 2**	**Test 3**
Time step [s]	1.1 10e-4	1.1 10e-4	1.1 10e-4
Initial time [s]	0	0	0
Duration [min]	40	40	40

Table 6: **Newmark solver** parameters for experiment number 3

A.4. Experiment number: 4

	Test 1	**Test 2**	**Test 3**
Type	Sine sweep	Sine sweep	Sine sweep
Forced dof(s)	1	1	1
Amplitude [N]	50	30	30
Starting frequency[Hz]	45	5	45
Ending frequency [Hz]	5	45	5
Phase	-	-	-
Sweep rate [Hz/min]	1	1	1
Sweep style	linear	linear	linear
Number of repetitions	-	-	-

Table 7: **External force** parameters for experiment number 4

	Test 1	**Test 2**	**Test 3**
Time step [s]	1.1 10e-4	1.1 10e-4	1.1 10e-4
Initial time [s]	0	0	0
Duration [min]	40	40	40

Table 8: **Newmark solver** parameters for experiment number 4

A.5. Experiment number: 5

	Test 1	**Test 2**	**Test 3**
Type	Sine	Sine	Sine
Forced dof(s)	1	1	1
Amplitude [N]	30	30	30
Starting frequency[Hz]	-	-	-
Ending frequency [Hz]	-	-	-
Phase	0	0	0
Sweep rate [Hz/min]	1	1	1
Sweep style	-	-	-
Number of repetitions	-	-	-
Forcing frequency [Hz]	40	30	10

Table 9: **External force** parameters for experiment number 5

	Test 1	**Test 2**	**Test 3**
Time step [s]	1.1 10e-4	1.1 10e-4	1.1 10e-4
Initial time [s]	0	0	0
Duration [min]	10	10	10

Table 10: **Newmark solver** parameters for experiment number 5